

Article

Catalytic Performance of MgO-Supported Co Catalyst for the Liquid Phase Oxidation of Cyclohexane with Molecular Oxygen

Mingzhou Wu, Yu Fu, Wangcheng Zhan *, Yanglong Guo, Yun Guo, Yunsong Wang and Guanzhong Lu *

Key Laboratory for Advanced Materials and Research Institute of Industrial Catalysis, School of Chemistry and Molecular Engineering, East China University of Science and Technology, Shanghai 200237, China; wumingzhou888@163.com (M.W.); yfyf1010@hotmail.com (Y.F.); ylguo@ecust.edu.cn (Y.G.); yunguo@ecust.edu.cn (Y.G.); yswang@ecust.edu.cn (Y.W.)

* Correspondence: zhanwc@ecust.edu.cn (W.Z.); gzhlu@ecust.edu.cn (G.L.); Tel.: +86-21-6425-2923 (W.Z.); +86-21-6425-2827 (G.L.)

Academic Editor: Véronique Nardello-Rataj

Received: 21 March 2017; Accepted: 9 May 2017; Published: 13 May 2017

Abstract: A highly-efficient and stable MgO-supported Co (Co/MgO) catalyst was developed for the oxidation of cyclohexane with oxygen. The effects of the Co loading and support on the catalytic activity of the supported Co_3O_4 catalyst were investigated. The results show that the Co supported on MgO presented excellent activity and stability. When the Co/MgO catalyst with the Co content of 0.2 wt % (0.2%Co/MgO) was used, 12.5% cyclohexane conversion and 74.7% selectivity to cyclohexanone and cyclohexanol (KA oil) were achieved under the reaction conditions of 0.5 MPa O_2 and 140 °C for 4 h. After being repeatedly used 10 times, its catalytic activity was hardly changed. Further research showed that the high catalytic performance of the 0.2%Co/MgO catalyst is attributed to its high oxygen-absorbing ability and the high ratio between the amount of weak and medium base sites with the help of the synergistic interaction between Co and MgO.

Keywords: MgO-supported Co catalyst; cyclohexane oxidation; oxygen oxidant; base sites

1. Introduction

The aerobic oxidation of cyclohexane is crucial in the chemical industry, because the products of this reaction—cyclohexanol and cyclohexanone (the mixture of the cyclohexanone and the cyclohexanol called KA oil in industry)—are important feedstock in a variety of reactions [1]. KA oil is also an indispensable intermediate for polyamide and plastics production, such as nylon 6 and nylon 66 [2–4]. Currently, the commercial production of cyclohexane oxidation is processed at about 150 °C under 1–2 MPa oxygen atmosphere over the homogeneous cobalt salt catalyst, in which a low conversion (~4%) is obtained to avoid the formation of side products and to obtain a high selectivity (~85%) toward KA oil [5]. Therefore, it is urgent to develop a new reaction process with a high cyclohexane conversion and high selectivity to KA oil.

To date, the varied reaction processes of cyclohexane oxidation have been exploited and can be distinguished by their different oxidants, mainly containing hydrogen peroxide (H_2O_2), *tert*-butyl hydroperoxide (TBHP) and oxygen. As a result, various kinds of catalysts have been developed based on the used oxidant and reaction system, such as metal coordination polymers [6–10], supported noble metals [11–16], supported metal complexes [17–20], metal doped-molecular sieves [21–23] and metal oxides [24–26]. There is great difference in the catalytic activity of the same catalyst for the cyclohexane oxidation under a different catalytic system. In general, the liquid reaction system using

hydrogen peroxide and *tert*-butyl hydroperoxide is inclined to achieve a high cyclohexane conversion. For example, 15.97% conversion of cyclohexane can be achieved using CrCoAPO-5 molecular sieves with H₂O₂ oxidant and acetone solvent at 90 °C [27]. However, only 5.9% conversion of cyclohexane was obtained with 1.0 MPa O₂ at 115 °C without any solvent using the CrCoAPO-5 catalyst [28]. However, due to ever-increasing environmental concerns, benign oxidation is urgently required for green chemistry, such as green oxidants, solvent-free reaction and heterogeneous catalysts. Hence, molecular oxygen as a kind of clean oxidant has garnered much more attention due to it being environmentally friendly and readily available in comparison to other oxidants [29].

The oxidation of cyclohexane without any solvent using O₂ as an oxidant is a gas–solid–liquid reaction system, in which the reactants are difficult to turn into a product, leading to low conversion of cyclohexane generally. Even though significant progress has been made in the oxidation of cyclohexane with O₂, a high conversion of cyclohexane and high selectivity to KA oil is still a challenge, in which the key problem is to develop a highly efficient catalyst that is environmentally benign, low-cost and with easy separation. Various heterogeneous catalysts were reported to be active in the oxidation of cyclohexane, mainly containing precious metals (Au, Pd) [11,12], modified molecular sieves (AlPO [30], Bi-MCM-41 [31], Au/ZSM-5 [29], Ce-HMS [23], etc.) and metal oxides [32–34]. Zhang et al. used Mn_{0.5}Ce_{0.5}O_x catalyst with mesoporous structure and rich porosity, which were in favor of fast mass transfer/diffusion and more active sites exposure, and 17.7% conversion of cyclohexane was obtained at 100 °C under 1.0 MPa O₂ with CH₃CN solvent for 12 h [24].

As is well-known, oxidation of cyclohexane follows the free radical mechanism [35], which requires plenty of surface defects on the catalyst to initiate the reaction. Therefore, metal oxides characterized by low cost, abundant surface hydroxyl and surface defects show potential application in the oxidation of cyclohexane. For example, 7.6% conversion of cyclohexane and selectivity of 89.1% to KA oil were achieved over the Co₃O₄ nanocrystals for cyclohexane oxidation with molecular oxygen [34]. In addition, the catalytic activity of Co₃O₄ could be improved by controlling its morphology and crystal face exposure. At the same time, its catalytic activity can also be enhanced by improving its surface area to increase the amount of active sites on the catalyst surface. For example, introducing Mn into Co₃O₄ to form Mn–Co mixed oxide can markedly enhance the catalytic activity and stability of Co₃O₄, over which 10.4% of cyclohexane conversion and 6.3% of KA oil yield were obtained [36].

In this paper, we prepared the Co₃O₄ supported on MgO catalysts for the oxidation of cyclohexane using molecular oxygen oxidant without any other solvent, and investigated the effects of the Co amount and the acid/base property of support on the physicochemical properties and catalytic performance of the Co₃O₄/MgO catalyst, and the improvement of its high catalytic performance by the synergistic effect between cobalt oxide and the MgO support. Using the hot filtration testing and recycle usage methods, the stability of the 0.2%Co/MgO catalyst was tested, and the results show that after being repeatedly used 10 times, the activity of this catalyst was hardly changed.

2. Results and Discussion

2.1. Effects of the Carrier and Co Loading

The effects of the carrier on the catalytic property of the 0.2% Co catalyst for the oxidation of cyclohexane are shown in Table 1. In the absence of any solvent with O₂ oxidant, it is found that the catalytic activity of blank support was much lower than that of the prepared catalysts. The activity of the supported catalysts followed in the order of Co/MgO > Co/BaCO₃ > Co/ZrO₂ ≈ Co/SAPO-34 > Co/Al₂O₃ > Co/TiO₂ > Co/SiO₂ on the basis of the KA oil yield. The stronger basicity the support has, the higher its catalytic activity was. These results indicate that the basicity of the carrier and the interfacial interaction between the support and Co₃O₄ are critical to obtain the high activity catalyst. The increase in basicity or the electron of the support could enhance the net negative charge density on the support surface, and benefit the positively charged Co dispersion on the surface of

the basic support. Similar phenomena were observed in the Al₂O₃, TiO₂, SiO₂ and MgO supported vanadium catalysts [37,38]. On the other hand, the increase in basicity of the support can accelerate the decomposition of intermediate product cyclohexyl hydroperoxide (CHHP) to cyclohexylperoxy radicals (ROO·). Subsequently, the propagation sequence can be enhanced, such as H abstraction from cyclohexane by ROO· to form CHHP accompanied by the formation of cyclohexyl radicals (R·). As a result, the activity of catalysts supported on the carrier with strong basicity for the oxidation of cyclohexane was improved [36]. Based on the results in Table 1, MgO was chosen as the support of the Co catalyst for cyclohexane oxidation.

Table 1. Oxidation of cyclohexane over an oxide support and supported by 0.2% Co catalysts ^a.

Catalyst	Conversion (%)	Selectivity (%)				Yield of KA (%)
		-nol (A) ^b	-none (K) ^b	KA oil	Acids	
Co/MgO	12.5	38.1	36.6	74.7	5.2	8.8
Co/BaCO ₃	10.1	40.5	37.9	78.4	5.0	7.9
ZrO ₂	5.3	39.3	36.8	76.1	5.5	4.0
Co/ZrO ₂	10.8	35.7	33.3	69.0	7.1	7.5
Co/SAPO-34	10.2	37.2	35.6	72.8	9.2	7.4
Al ₂ O ₃	4.8	32.3	35.0	67.3	4.8	3.2
Co/Al ₂ O ₃	9.5	34.9	35.4	70.3	8.3	6.7
TiO ₂	1.5	39.1	43.5	82.6	5.9	1.2
Co/TiO ₂	8.1	37.8	39.2	77.0	7.9	6.2
SiO ₂	1.1	41.6	45.4	87.0	3.1	1.0
Co/SiO ₂	6.8	39.5	41.2	80.7	9.5	5.5

^a Reaction conditions: 4.0 g of cyclohexane, 20 mg catalyst, initial 0.5 MPa O₂, at 140 °C for 4 h; ^b -nol and -none denote the cyclohexanol and cyclohexanone.

Table 2 shows the catalytic performance of the MgO, Co₃O₄ and Co/MgO catalysts. By the GC-MS analysis, the main by-products were hexanoic acid, dicyclohexyl adipate, cyclohexyl caproate and adipic acid. As shown in the table, 1.1% conversion and 90.8% selectivity to KA oil were reached after reaction in the blank system without any catalyst. Over the pure MgO support, only 1.3% conversion of cyclohexane and 88.1% selectivity to KA oil were achieved, and in the N₂ atmosphere, the oxidation products could not be detected, due to the absence of the oxidant. For the Co/MgO catalysts, their catalytic activities (based on the KA oil yield) were ranked in the order of 0.2%Co/MgO > 5.0%Co/MgO > 0.5%Co/MgO ≈ 1.0%Co/MgO > 3.0%Co/MgO > 0.1%Co/MgO > MgO. The catalytic activity of the 0.2%Co/MgO with 12.5% conversion of cyclohexane and 74.7% selectivity to KA oil was much higher than that of the physical mixture of Co₃O₄ and MgO catalyst (a conversion and selectivity of 6.1% and 64.5%). However, when air was used as an oxidant instead of O₂, the conversion of cyclohexane and the selectivity to KA oil on the 0.2%Co/MgO declined to 3.2% and 90.1% in 0.5 Mpa air atmosphere, due to the decrease in the O₂ pressure in the reaction system. These results indicate that Co₃O₄ supported on MgO is the main active component for the oxidation of cyclohexane, and 0.2%Co/MgO is an efficacious catalyst for cyclohexane oxidation using O₂ oxidant. The Co dispersion (D_{Co}) of the 0.2%Co/MgO was 7.5%, which was measured by the O₂ pulse chemisorption [39]. TOF (turnover frequency) of 0.2%Co/MgO was calculated to be 8.2 s⁻¹ by TOF = $\Delta n_{ane} / (n_{Co} \times D_{Co} \times T)$ (-ane denotes the cyclohexane; Δn_{ane} —the converted cyclohexane (mol); n_{Co} —the Co amount in the catalyst (mol); T—the reaction time (s)). As shown in Table 2, compared with the Co-TUD-1 [40] and Au/MgO catalysts [35], the 0.2%Co/MgO catalyst exhibits higher catalytic activity for the oxidation of cyclohexane under similar reaction conditions.

Other researchers reported that a free-radical initiator (for example, TBHP) can improve the catalytic activity of the catalyst by accelerating the auto-oxidation process at the initiation stage using O₂ oxidant [34]. Here, the effect of TBHP on the oxidation reaction over the 0.2%Co/MgO catalyst was also examined. As shown in Table 2, in the presence of TBHP, the conversion of cyclohexane was increased to 15.6%, and the yield of KA oil reached 10.5%. However, in the presence of the free-radical scavenger (hydroquinone), the process of oxidation was almost forced to stop, that is to say, this reaction procedure based on the free radical mechanism [41].

Table 2. Catalytic performances of the MgO, Co₃O₄ and Co/MgO catalysts for the oxidation of cyclohexane ^a.

Catalyst	Temp./Time (°C h ⁻¹)	Pressure (MPa)	Conversion (%)	Selectivity (%)			Y _{KA} (%)	Mass Balance ^c (%)
				-nol (A)	-none (K)	Acids ^b		
Blank	140/5	O ₂ /0.5	1.2	43.0	49.2	4.1	1.1	95
MgO	140/4	O ₂ /0.5	1.3	40.2	47.9	3.4	1.1	94
MgO	140/4	N ₂ /0.5	-	-	-	-	-	-
0.1%Co/MgO	140/4	O ₂ /0.5	8.2	40.3	38.1	4.2	6.4	95
0.2%Co/MgO	140/4	air/0.5	3.2	47.5	42.6	2.7	2.9	96
0.2%Co/MgO	140/4	O ₂ /0.5	12.5	38.1	36.6	5.2	9.3	-
0.2%Co + MgO ^d	140/4	O ₂ /0.5	6.1	35.7	28.8	5.0	4.6	-
0.2%Co/MgO ^e	140/4	O ₂ /0.5	15.6	34.7	32.5	6.3	10.5	-
0.2%Co/MgO ^f	140/4	O ₂ /0.5	-	-	-	-	-	-
0.5%Co/MgO	140/4	O ₂ /0.5	12.0	36.4	34.6	9.6	8.5	95
1.0%Co/MgO	140/4	O ₂ /0.5	12.6	34.4	33.0	6.3	8.5	95
3.0%Co/MgO	140/4	O ₂ /0.5	11.7	34.2	32.8	4.5	7.9	94
5.0%Co/MgO	140/4	O ₂ /0.5	13.3	33.2	31.9	5.3	8.7	95
Co ₃ O ₄	140/4	O ₂ /0.5	7.7	44.2	22.4	10.2	5.1	95
Au/MgO g of [35]	140/17	O ₂ /0.3	5.0	50	29	19	4.0	-
Co-TUD-1 ^h [40]	120/24	8%O ₂ /N ₂ /1.5	3.8	56	31	-	3.3	-

^a Reaction conditions: 4.0 g of cyclohexane, 20 mg catalyst, initial 0.5 Mpa O₂; ^b main byproducts: Adipic acid and hexanoic acid; ^c mass balance is equal to the weight ratio of (the products)/(the reaction mixture) without the catalyst; ^d physical mixture of Co₃O₄ and MgO; ^e adding a small amount (3 wt % cyclohexane) of *tert*-butyl hydroperoxide (free-radical initiator); ^f adding a small amount (3 wt % cyclohexane) of hydroquinone (free-radical scavenger); g of reaction conditions: 10 mL cyclohexane, 0.05 mmol *tert*-butylhydroperoxy (radical initiator), 6 mg catalyst; ^h TUD-1 is mesoporous molecular sieve; reaction conditions: 175 mmol cyclohexane, 0.05 mmol cyclohexyl hydroperoxide (radical initiator), 0.1 mmol active metal species.

2.2. Structure and Surface Properties

XRD (X-ray powder diffraction). As shown in Figure 1, there are diffraction peaks of MgO at $2\theta = 37.0, 42.9, 62.3, 74.7,$ and 78.7° (JCPDS No. 45-0946) for all the samples. With the increase in the Co loading, the diffraction peaks of MgO weakened gradually. In the XRD patterns of the Co/MgO catalysts, even though the Co loading reached 5.0%, the diffraction peaks of Co₃O₄ and CoO were not observed, due to high dispersion of Co on the MgO support. The crystallite size of the catalysts was calculated on the basis of the diffraction peak of (200) plane by the Scherrer formula. As shown in Table 3, MgO exhibited the biggest crystallite size (36.6 nm), and after Co oxide was supported, the crystallite sizes of the Co/MgO became smaller. With increasing Co amount, the crystallite size of the Co/MgO catalyst increased and then decreased, and 1.0%Co/MgO possessed the biggest crystallite size (24.5 nm). For the d_{200} spacing and cell parameter (a_0), there is no obvious difference between the MgO support and Co/MgO samples with a different Co amount. However, after supporting Co on the MgO support, its BET (Brunner–Emmet–Teller measurement) surface area was increased from 15.0 to 58.7 m² g⁻¹ (0.2%Co/MgO), then gradually decreased from 58.7 to 41.2 m² g⁻¹ with the increase in the Co amount from 0.2% to 3.0%. When the Co amount was increased to 5.0%, the surface area of 5%Co/MgO instead increased to 51 m²/g, due to its smaller crystallite size (12.4 nm).

Table 3. BET surface area (S_{BET}), and the crystal parameters of the MgO and Co/MgO catalysts.

Sample	S _{BET} (m ² g ⁻¹)	Co Content ^a (wt %)	Crystallite Size ^b (nm)	d_{200} Spacing (nm)	a_0 ^c (nm)
MgO	15.0	-	36.6	2.106	4.21
0.2%Co/MgO	58.7	0.2	21.1	2.105	4.21
0.5%Co/MgO	49.3	0.5	22.8	2.103	4.21
1.0%Co/MgO	43.4	1.0	24.5	2.108	4.22
3.0%Co/MgO	41.2	3.0	23.4	2.104	4.21
5.0%Co/MgO	51.0	5.0	12.4	2.109	4.22

^a Co content in the bulk was determined by ICP-AES (inductively coupled plasma atomic emission spectroscopy);

^b Crystallite size was calculated by the Scherrer equation on the basis of the diffraction peak of (200) plane; ^c Cell parameter (a_0) was calculated by $a_0 = d_{200} (4)^{1/2}$.

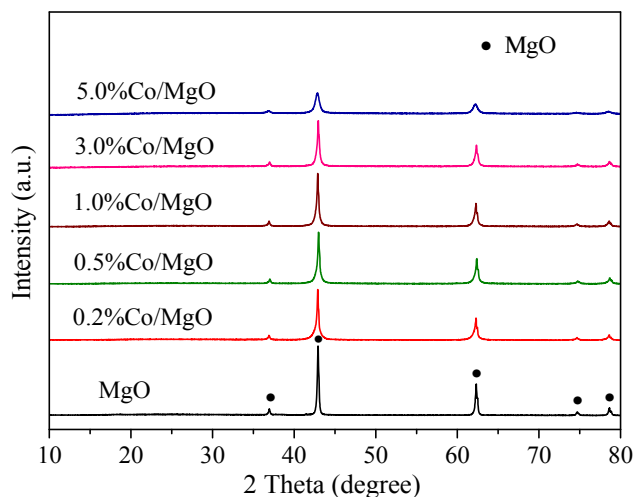


Figure 1. XRD patterns of the MgO and Co/MgO catalysts.

Co laser Raman spectroscopy (LRS). LRS is usually used to measure the surface properties of solid materials, especially for transition metal oxides, because it is able to sensitively probe the bonds of solid material and the surface structures by analyzing their vibration spectra. Laser Raman spectra of the MgO and Co/MgO catalysts are shown in Figure 2. The Raman spectrum of MgO did not show any characteristic bands in the region of $100\sim 1500\text{ cm}^{-1}$ [42]. The band at 1100 cm^{-1} can be attributed to a disorder-induced two-phonon band [43], and is obvious in the Raman spectrum of 0.2%Co/MgO compared with other Co/MgO samples. Some vibration bands at $569\sim 582\text{ cm}^{-1}$ appeared in the Raman spectra of 3%~5%Co/MgO catalysts and resulted from the substitution of Co ions by Mg ions in the solid [44]. The band at $660\sim 680\text{ cm}^{-1}$ is the characteristic band of the octahedral sites (CoO_6) and is assigned to the A_{1g} symmetry mode in the O_h^7 spectroscopic space group [45,46]. The weak band at 189 cm^{-1} of the 5%Co/MgO catalyst is attributed to the characteristic vibration mode of F_{2g}^3 symmetry from the tetrahedral sites (CoO_4). For the A_{1g} vibration mode, it shifts toward lower wavenumber with the increase in the Co amount, which indicates the highly defective structure in Co oxide [47,48]. Therefore, the Co/MgO catalysts are partially covered by Co oxide, and the surface defects are increased by increasing the Co amount from 3% to 5%, which is beneficial to the higher activity of the 5%Co/MgO catalyst compared with the 3%Co/MgO catalyst.

XPS (X-ray photoelectron spectroscopy). The XPS O 1s, Mg 1s and Co 2p spectra of the Co/MgO samples are shown in Figure 3. Table 4 shows the surface composition of the Co/MgO samples based on the XPS data. The results show that all Co/MgO catalysts exhibited a similar XPS O 1s spectra, in which two sub-peaks can be resolved at binding energy of $\sim 529.4\text{ eV}$ and $\sim 531.2\text{ eV}$. The peak located at lower binding energy corresponds to the lattice oxygen O^{2-} (O_{lat}), and the one at higher binding energy can be assigned to O_{ads} that includes the surface oxygen (O_2^{2-} or O^-) belonging to the defective oxide or hydroxyl-like group and weakly bonded oxygen species [49–51]. The ratio of $\text{O}_{\text{ads}}/(\text{O}_{\text{lat}} + \text{O}_{\text{ads}})$ on the Co/MgO samples is similar except for the 0.5%Co/MgO sample, as shown in Table 1. The 0.5%Co/MgO sample shows the lowest ratio of $\text{O}_{\text{ads}}/(\text{O}_{\text{lat}} + \text{O}_{\text{ads}})$ of 0.47. To a certain extent, this trend is opposite to their activity for cyclohexane oxidation. In the XPS Mg 1s spectra of the Co/MgO samples, there is only one peak at binding energy of 1304.4 eV , and no obvious difference can be observed with the increase in the Co amount. Because of the low Co amount, no peak was shown in the XPS Co 2p spectrum of the 1.0%Co/MgO sample. However, the 3.0%Co/MgO and 5.0%Co/MgO samples exhibit two peaks assigned to Co^{3+} and Co^{2+} at binding energy of 780.6 eV and 782.0 eV , respectively. In addition, the peak at about 787.4 eV is the satellite peak of Co 2p [52,53]. Compared with the atomic ratios of Co^{3+}/Co (0.7) and $\text{Co}^{3+}/\text{Co}^{2+}$ (2.0) on the surface of the 5.0%Co/MgO catalyst, the corresponding values of the 3.0%Co/MgO catalyst are 0.6 and 2.0. These results indicate

the same valence state of Co in the 3.0%Co/MgO and 5.0%Co/MgO samples. Therefore, the difference in their catalytic activities is due to other structure factors.

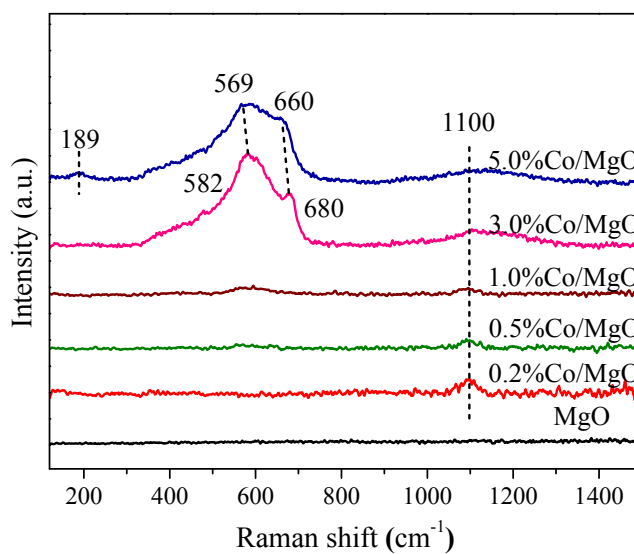


Figure 2. Laser Raman spectra of the MgO and Co/MgO catalysts.

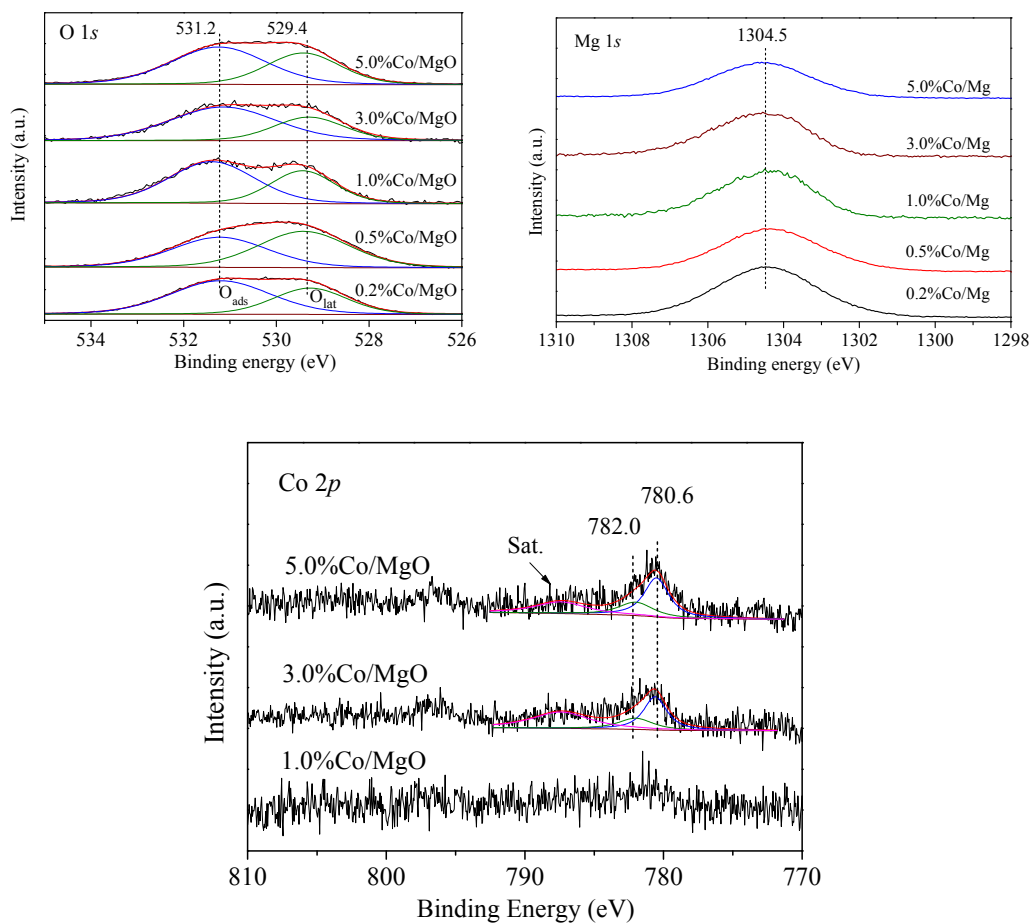


Figure 3. XPS O 1s and Mg 1s spectra of 0.2%Co/MgO, 0.5%Co/MgO and 5.0%Co/MgO; Co 2p spectra of 1.0%Co/MgO, 3.0%Co/MgO and 5.0%Co/MgO.

Table 4. Compositions of the 0.2%Co/MgO, 0.5%Co/MgO and 5.0%Co/MgO samples determined by XPS.

Sample	Surface Atom Concentration (%)		Mg/O (Atom)	Co ³⁺ /Co Atomic Ratio	Co ³⁺ /Co ²⁺ Atomic Ratio	O _{ads} /(O _{ads} + O _{lat})
	Mg	O				
0.2%Co/MgO	29.6	49.5	0.60	-	-	0.63
0.5%Co/MgO	28.8	51.8	0.56	-	-	0.47
1.0%Co/MgO	34.6	65.4	0.53	-	-	0.63
3.0%Co/MgO	33.4	66.6	0.50	0.6	2.0	0.65
5.0%Co/MgO	22.8	51.9	0.44	0.7	2.0	0.60

2.3. Surface Basic Property (Temperature Programmed Desorption of CO₂ (CO₂-TPD))

CO₂-TPD was used to investigate the surface basicity of the Co/MgO catalysts and the CO₂-TPD results of the MgO and Co/MgO samples are shown in Figure 4a. In the CO₂-TPD pattern of the MgO support, there are three CO₂ desorption peaks (α at 75 °C, β at 160 °C, γ at 235 °C) at <400 °C, which can be assigned as different kinds of basic sites with two strengths, i.e., “weak” (30~115 °C), “medium” (115~375 °C) basic sites; the desorption peak at >400 °C is ascribed to the “strong” basic sites. The “weak” sites probably correspond to Brønsted basicity, which most likely originates from the hydroxyl groups on the surface. The “medium” and “strong” sites are most likely associated with Lewis basicity which resulted from the three- and four-fold-coordinated O²⁻ anions [48]. As is well-known, the surface of most oxides is hydroxylated due to the dissociative chemisorption of water [54].

After cobalt oxide was loaded onto the MgO support, the positions of desorption peaks are hardly changed, this is to say, the surface acidic strength on the Co/MgO is unchanged, but their peak areas are increased obviously, which may be ascribed to the increase in the surface area with increasing Co amount (Table 3). At this stage, the numbers of the weak and medium base sites per square meter were calculated and the results are listed in Table 5. With the increase in the Co loading, the weak base density (a.u. m⁻²) per square meter is decreased from 4.7 to 3.2 a.u. m⁻² except for the 5.0%Co/MgO catalyst (5.2 a.u. m⁻²); for the medium base sites, there is no obvious change tendency. The ratios of weak base/medium base and weak base/(weak + medium) base were ranked in the order of 0.2%Co/MgO > 5.0%Co/MgO > 0.5%Co/MgO > 1.0%Co/MgO > 3.0%Co/MgO > MgO. The trends of KA oil yield and the ratio of weak base/medium base are shown in Figure 4b, and the consistency between them is illustrated. Therefore, the relative amount of weak base sites compared with medium base sites is one of the key parameters that influences the catalytic activity of the Co/MgO catalyst for the oxidation of cyclohexane.

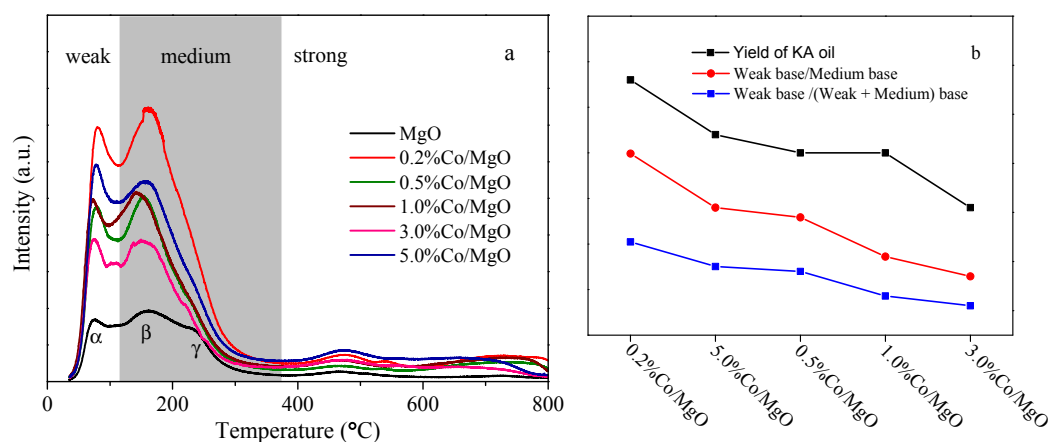
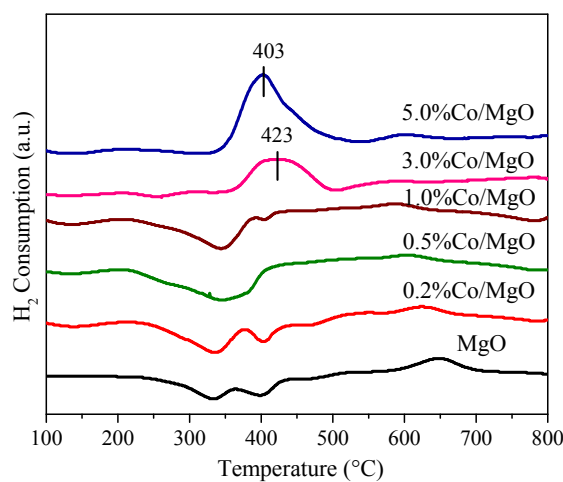
**Figure 4.** CO₂-TPD profiles of the MgO and Co/MgO catalysts (a) and trends between KA yield and weak base ratio (b).

Table 5. The numbers (a.u. m⁻²) of the weak and medium base sites per square meter on MgO and Co/MgO.

Sample	Weak Base (a.u. m ⁻²)	Medium Base (a.u. m ⁻²)	Weak Base/Medium Base	Weak Base/(Weak + Medium) Base
MgO	4.7	23.2	0.20	0.17
0.2%Co/MgO	4.7	9.0	0.52	0.34
0.5%Co/MgO	4.5	11.4	0.39	0.28
1.0%Co/MgO	4.3	14.1	0.31	0.23
3.0%Co/MgO	3.2	11.9	0.27	0.21
5.0%Co/MgO	5.2	12.7	0.41	0.29

2.4. Redox Property (*H*₂ Temperature-Programmed Reduction (*H*₂-TPR) and Temperature Programmed Desorption of O₂ (O₂-TPD))

The *H*₂-TPR profiles of the MgO and Co/MgO samples are shown in Figure 5. Note that there are two negative peaks at ~330 °C and ~400 °C in the *H*₂-TPR profiles of the MgO, 0.2%Co/MgO, 0.5%Co/MgO and 1.0%Co/MgO catalysts, which could be attributed to the release of *H*₂ adsorbed on the catalyst surface, because MgO is an excellent hydrogen storage material [55]. When the Co loading was ≤1.0%, the Co₃O₄ reduction peaks could not be observed, which is probably because the amount of hydrogen released from MgO is much greater than the amount of hydrogen consumed for the Co₃O₄ reduction. In the TPR profiles of the 3.0%Co/MgO and 5.0%Co/MgO catalysts, there is a similar reduction peak at 350 °C~500 °C, which is ascribed to the reduction of Co₃O₄ [37,48,56]. Its *H*₂ consumption amount is increased with the increase in the Co amount. Compared with the 3.0%Co/MgO catalyst, the reduction peak of the 5.0%Co/MgO catalyst moves to a lower temperature. This result indicates the better reduction property of 5.0%Co/MgO, which is favorable to improve its catalytic activity, since the decomposition of reaction intermediate cyclohexyl hydroperoxide (CHHP) is proposed to involve one-electron redox cycles [26,30].

**Figure 5.** *H*₂-TPR profiles of the MgO and Co/MgO catalysts.

In the O₂-TPD profiles of 0.2%Co/MgO, 0.5%Co/MgO, 1.0%Co/MgO and 3.0%Co/MgO (Figure 6), there are two broad peaks at 95~500 °C, and only one peak is observed at <290 °C for the 5.0%Co/MgO sample. Generally, the difficulty in desorption of oxygen species from the catalyst is in the following sequence: O₂ (ad) < O₂⁻ (ad) < O⁻ (ad) < O²⁻ (lattice) [57,58]. In the O₂-TPD profiles over the Co/MgO catalysts, the desorption peaks below 95 °C are assigned to physically adsorbed oxygen, and the α peak at 95~290 °C can be ascribed to chemically adsorbed oxygen O₂ (ad) or O₂⁻ (ad) species [58]. The β peak at 290~500 °C can be ascribed to weak surface lattice oxygen O²⁻ (surface)

and chemically adsorbed oxygen O^- (ad) on the vacancies. Besides, bulk lattice oxygen O^{2-} (lattice) can be desorbed at high temperature ($> 750\text{ }^\circ\text{C}$) [59]. More attention should be paid to the α and β peaks because only chemically adsorbed oxygen and surface lattice oxygen can participate in the oxidation reaction. When the Co amount was increased to 5.0%, its α peak reached the maximum value (5.2, a.u. peak area). For the β peak, it was decreased with the increase in the Co amount. The total area of α and β peaks is decreased in the order of 0.2%Co/MgO (9.8) $>$ 0.5%Co/MgO (5.7) \approx 1.0%Co/MgO (5.5) $>$ 3.0%Co/MgO (4.8), which coincides with the change order of the catalytic activity shown in Table 2.

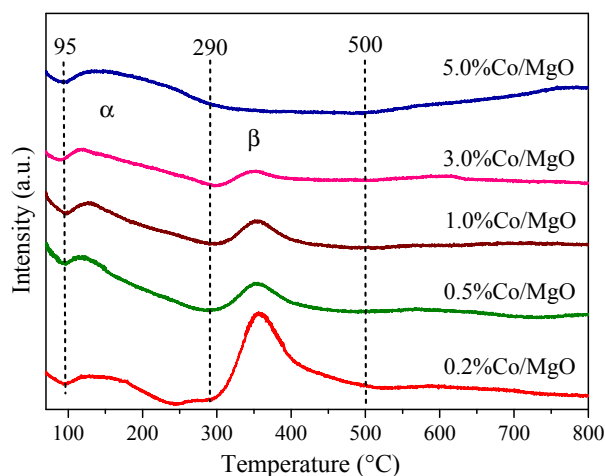


Figure 6. O_2 -TPD profiles of the Co/MgO catalysts.

2.5. SEM (scanning electron microscope) and TEM (transmission electron microscope) Images

The SEM images of the catalysts are shown in Figure 7. The 0.2%Co/MgO and 5.0%Co/MgO catalysts exhibited a similar and sheet-like morphology with a clear boundary and interconnection; with the increase in the Co amount, many pores developed in the sheet crystallites, which shows that the sheets consisted of many small particles by aggregation. In the TEM image of 0.2%Co/MgO (Figure 8a), the Co_3O_4 was well dispersed on the MgO surface with a tiny (0.2%) Co amount, which meant that the lattice fringes of the Co_3O_4 could not be observed during the TEM measurement; the stripe type particles with $30\sim 50\text{ nm} \times 100\text{ nm}$ should result from the MgO support. In comparison with the 0.2%Co/MgO catalyst, the 5.0%Co/MgO sample exhibited smaller Co_3O_4 particles, consistent with the crystallite size (Table 3). However, the interplanar spacings of 0.46 nm and 0.20 nm, assigned to the (111) and (400) planes of Co_3O_4 , can be observed in HTEM (high resolution transmission electron microscopy) image of 5%Co/MgO catalyst [60,61].

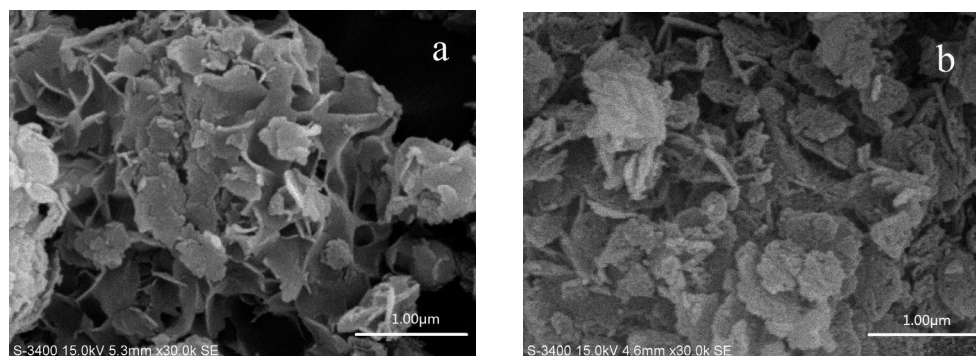


Figure 7. SEM images of the (a) 0.2%Co/MgO and (b) 5.0%Co/MgO catalysts.

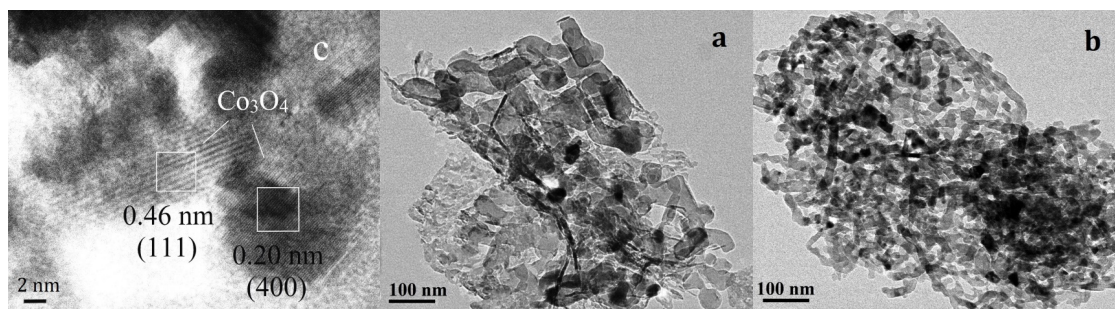


Figure 8. TEM images of the (a) 0.2%Co/MgO and (b,c) 5.0%Co/MgO catalysts.

2.6. The Stability of the 0.2%Co/MgO Catalyst

Firstly, the hot filtration experiment was adopted to test the stability of the 0.2%Co/MgO catalyst [62]. The reaction solution was filtered after 1.5 h of reaction, and then kept at 140 °C for a further 2.5 h under the same conditions. It was found that the cyclohexane conversion in the filtrate was slightly increased from 6.0% to 6.5%, which is much lower than that (12.5%) over the catalyst at 140 °C for 4 h.

Subsequently, the catalytic performance of the recycled 0.2%Co/MgO catalyst was tested with the same procedure as its first reaction, and the results for repeated usage (10 times) are shown in Figure 9. It is found that the cyclohexane conversion and the selectivity of KA oil are hardly changed after being repeatedly used 10 times. This research indicates the relative stability of the 0.2%Co/MgO catalyst for the oxidation of cyclohexane. After the first run, the contents of Co and Mg were measured to be 0.62 ppm and 0.78 ppm in the reaction solution by inductively coupled plasma atomic emission spectroscopy (ICP-AES), which indicates barely any Co and Mg loss during the reaction. Further, analysis of the mass ratio of Co/Mg in the 0.2%Co/MgO catalyst by ICP-AES showed that the Co loading is the same as the fresh catalyst after being repeatedly used 10 times, that is, 0.2%Co on MgO is not varied.

Unfortunately, as shown in the TEM/SEM images (Figure 10), the structure and morphology of the 0.2%Co/MgO catalyst have been changed to some degree, because the regenerated catalyst was calcinated at 500 °C for 2 h after every run. However, the diffraction peaks of Co_3O_4 and CoO were still not observed in the XRD pattern (Figure 10) of the catalyst after the tenth recycling cycle, indicating a high dispersion of Co on the MgO support. That is the reason why the activity of the regenerated catalyst for cyclohexane oxidation can be retained.

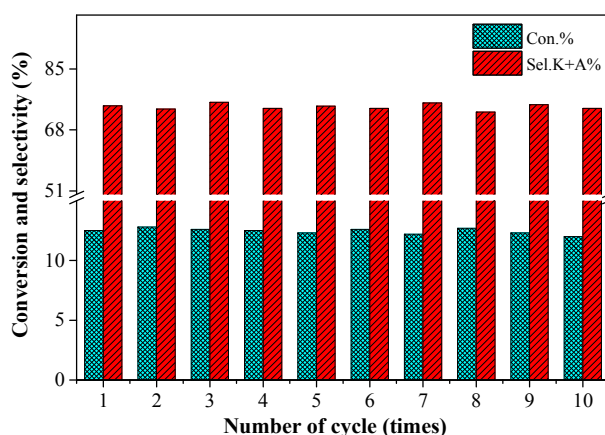


Figure 9. The recycling tests on the catalytic activity of 0.2%Co/MgO for the cyclohexane oxidation. Reaction conditions: 4.0 g of cyclohexane, 20 mg catalyst, initial 0.5 MPa O_2 , at 140 °C for 4 h.

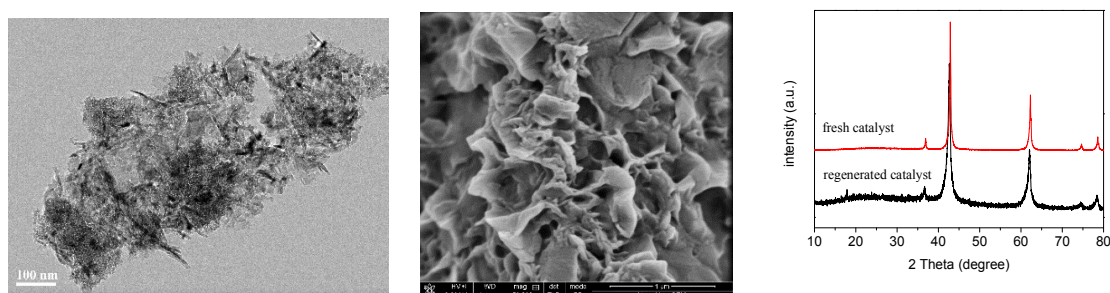


Figure 10. TEM (left) and SEM (middle) images, as well as XRD pattern (right) of the regenerated catalyst after the tenth recycling cycle.

3. Materials and Methods

3.1. Synthesis of Catalysts

The MgO-supported Co catalysts with different Co content were synthesized by the incipient impregnation method whilst controlling the dosage of $\text{Co}(\text{NO}_3)_2 \cdot 6\text{H}_2\text{O}$ (Sinopharm Chemical Reagent Co., Ltd., Beijing, China). The prepared catalysts were kept in an 80 °C drying oven overnight, followed by calcination at 500 °C for 4 h in static air. The obtained catalysts were designed as $x\%\text{Co}/\text{MgO}$, where x was the Co content in the prepared catalysts determined by inductively coupled-plasma atomic emission spectroscopy, i.e., 0.2, 0.5, 1.0, 3.0 or 5.0.

The MgO support was purchased from Sinopharm Chemical Reagent Co. Ltd. ZrO_2 (Sinopharm Chemical Reagent Co., Ltd., Beijing, China), TiO_2 (Sinopharm Chemical Reagent Co., Ltd., Beijing, China), BaCO_3 (Sinopharm Chemical Reagent Co., Ltd., Beijing, China), SiO_2 (Sinopharm Chemical Reagent Co., Ltd., Beijing, China), Al_2O_3 (commercial, Jiangyan, China), and SAPO-34 (commercial, Shanghai, China) were used as the support materials, and the 0.2%Co/support catalysts were prepared with the same procedure as the Co/MgO catalyst.

Co_3O_4 was prepared by the precipitation method with the $\text{Co}(\text{NO}_3)_2 \cdot 6\text{H}_2\text{O}$ aqueous solution and the NaOH (Sinopharm Chemical Reagent Co., Ltd., Beijing, China) aqueous solution as the precipitant. Typically, 1 M NaOH solution was dropped to 200 mL 0.2 M $\text{Co}(\text{NO}_3)_2$ solution under stirring until the pH of the synthesis solution was 8. After this synthesis solution was stirred for 6 h, the formed solids were collected by filtration, dried within a 120 °C oven, and kept for 4 h in a 500 °C furnace in the air atmosphere. A physical mixture of 0.2%Co and MgO was prepared by Co_3O_4 (equivalent 0.2 wt % Co) and MgO.

3.2. Characterization of Catalysts

The XRD characterization was obtained by a Bruker D8 Focus X-ray diffractometer equipped with $\text{CuK}\alpha$ radiation ($\lambda = 0.15406$ nm). N_2 adsorption–desorption isotherms were conducted on an ASAP 2010 equipment (Micromeritics Co., Ltd., Atlanta, GA, USA). Scanning electron microscope (SEM) photos were obtained on a JSM-6360LV microscope (JEOL, Tokyo, Japan). Transmission electron microscopy (TEM) photographs were obtained by a JEM-2100 (JEOL, Tokyo, Japan) instrument, and the catalyst was dispersed on a copper grid in ethanol solution. The bulk composition of the catalyst was measured by inductively coupled plasma atomic emission spectroscopy (ICP) analysis on an Agilent 725 ES instrument (Palo Alto, CA, USA). Laser Raman spectra (LRS) were collected through a Renishaw spectrometer adopted with a 514-nm line of a Spectra Physics Ar^+ laser.

H_2 temperature-programmed reduction (H_2 -TPR) curves were tested on a PX200 apparatus (Tianjin Golden Eagle Technology Limited Corporation, Tianjin, China) and detected by TCD (thermal conductivity detector). The catalyst of 50 mg was heated to 800 °C at 10 °C min^{-1} in the 5 vol % H_2/N_2 reduction atmosphere with a gas flow rate of 45 mL min^{-1} .

Temperature programmed desorption of CO₂ (CO₂-TPD) and O₂-TPD were conducted on a conventional flow system equipped with a U-shape quartz reactor and a mass spectrometer (HIDEN HPR 20, Warrington, England). A 100-mg sample was used and pre-treated in He (50 mL min⁻¹) at 400 °C for 30 min followed by cooling to ambient temperature. The catalyst was exposed to CO₂ (50 mL min⁻¹) or 3 vol % O₂/He (50 mL min⁻¹) for 1 h, and then purged with He for 1 h at ambient temperature. The catalyst was then heated from ambient temperature to 800 °C at a speed of 10 °C min⁻¹ under He flow gas (50 mL min⁻¹). The desorption amount of CO₂/O₂ was detected by the mass spectrometer.

3.3. Catalytic Activity Testing

The catalytic procedure of cyclohexane oxidation was carried out in a stainless-steel batch tank reactor (50 mL) equipped with an explosion-proof pressure sensor and a magnetic stirrer [63]. A 20-mg catalyst (~3000 mesh) and 4.0 g of cyclohexane were added to the reactor. After purging with oxygen three times, the reactor was charged to 0.5 MPa and then heated to 140 °C under stirring at a speed of 800 rpm and maintained for 4 h. In some cases, hydroquinone (free-radical scavenger) and *tert*-butyl hydroperoxide (TBHP, free-radical initiator) were used by adding them into the reaction system. Under the conditions of 4.0 g of cyclohexane, 20 mg catalyst, 140 °C and 0.5 MPa O₂, the effect of the diffusion on the conversion of cyclohexane was excluded by changing the granular size of the catalyst and rotation speed, that is to say, the oxidation reaction occurred in the kinetics control region.

After the autoclave was thoroughly cooled, a certain amount of ethanol was added to the product mixture to dissolve all of the by-products, followed by separation of the catalyst with centrifugation. An amount of 0.25 g of methylbenzene was added to the reaction mixture as an internal standard substance. Excess triphenylphosphine (PPh₃) was used to decompose cyclohexyl hydroperoxide (CHHP) to cyclohexanol in a mixture solution before analysis because of the easy decomposition of CHHP in the GC injector [64,65]. The remaining amount of cyclohexane and the main resultant cyclohexanol and cyclohexanone were quantified by an Agilent gas chromatograph (7890B) assembled with a FID (flame ionization detector) and HP-5 column. Other products were further identified by GC-MS (Agilent 7890A-5975C, Palo Alto, CA, USA). Formed acids were titrated by 0.1 M NaOH aqueous solution.

The conversion of cyclohexane (X), the selectivity (S) to cyclohexanol (A) or cyclohexanone (K) and the yield (Y) of KA oil were calculated by the following formulas:

$$X = \frac{n_{-ane}(\text{substrate}) - n_{-ane}(\text{residual})}{n_{-ane}(\text{substrate})} \times 100\% \quad (1)$$

$$S_{-nol(or-none)} = \frac{n_{-nol(or-none)}}{n_{-ane}(\text{substrate}) - n_{-ane}(\text{residual})} \times 100\% \quad (2)$$

$$Y_{KA} = (S_{-nol} + S_{-none}) \times X \quad (3)$$

where n_{-nol} and n_{-none} denote the mole amount of cyclohexanol and cyclohexanone in the products mixture. n_{-ane} (substrate) and n_{-ane} (residual) refer to the mole amount of cyclohexane substrate and the remaining amount in the system, respectively.

3.4. Repeated Usage of the Catalyst

The 0.2%Co/MgO sample was collected from the mixture by filtration after each reaction. After being washed with ethyl alcohol three times under stirring, the catalyst was dried at 80 °C and calcined in atmosphere at 500 °C for 2 h, obtaining our regenerated catalyst. If necessary, the regenerated catalyst was supplemented with live catalyst, and the activity property of the regenerated catalyst was tested under the same operational process as the live catalyst.

4. Conclusions

In summary, changing the Co loading (0.2~5 wt %) and support would affect the bulk compositions, surface areas, surface oxygen species, basicity and reactivity of supported Co oxide catalyst. Furthermore, for the cyclohexane oxidation by oxygen, alkaline MgO is an appropriate support for Co₃O₄, and its catalytic activity was ranked in the order of 0.2%Co/MgO > 5.0%Co/MgO > 0.5%Co/MgO ≈ 1.0%Co/MgO > 3.0%Co/MgO > MgO, which is the same as the rank for the ratios of weak base/medium base and weak base/(weak + medium) base of the Co/MgO catalysts, and similar to the change tendency for their ratio of O_{ads}/(O_{ads} + O_{lat}) calculated by the XPS data and the oxygen-absorbing ability. Over the 0.2%Co/MgO catalyst, conversion of cyclohexane up to 12.5% and selectivity to KA oil up to 74.7% can be achieved at 140 °C reacted for 4 h, and its TOF reached 8.2 s⁻¹, which is higher than the results reported. After being repeatedly used 10 times, the activity of the 0.2%Co/MgO catalyst was hardly changed, showing that this catalyst has good operational stability. The high catalytic performance of the 0.2%Co/MgO catalyst should be attributed to its high oxygen-absorbing ability and the high ratio between the amount of weak and medium base sites with the help of the synergistic interaction between Co and MgO.

Acknowledgments: This project was supported financially by the National Natural Science Foundation of China (91545103, 21103048) and the Fundamental Research Funds for the Central Universities (222201717003).

Author Contributions: G.L. and W.Z. conceived and designed the experiments; M.W. and Y.F. performed the experiments. M.W. and W.Z. analyzed the data; M.W. wrote the manuscript; Y.G., Y.G. and Y.W. contributed reagents/materials/analysis tools; M.W., W.Z. and G.L. modified the paper.

Conflicts of Interest: The authors declare no conflict of interest.

References

1. Clerici, M.G.; Kholdeeva, O.A. *Liquid Phase Oxidation via Heterogeneous Catalysis: Organic Synthesis and Industrial Applications*; John Wiley & Sons: Hoboken, NJ, USA, 2013; ISBN: 1118356756.
2. Schuchardt, U.; Carvalho, W.A.; Spinacé, E.V. Why is it interesting to study cyclohexane oxidation? *Synlett* **1993**, *1993*, 713–718. [[CrossRef](#)]
3. Sakthivel, A.; Selvam, P. Mesoporous (Cr)MCM-41: A mild and efficient heterogeneous catalyst for solvent oxidation of cyclohexane. *J. Catal.* **2002**, *211*, 134–143. [[CrossRef](#)]
4. Gómez-Hortigüela, L.; Corà, F.; Catlow, C.R.A. Aerobic oxidation of hydrocarbons catalyzed by Mn-doped nanoporous aluminophosphates(I): Preactivation of the Mn sites. *ACS Catal.* **2010**, *1*, 18–28. [[CrossRef](#)]
5. Schuchardt, U.; Cardoso, D.; Sercheli, R.; Pereira, R.; de Cruz, R.S.; Guerreiro, M.C.; Mandelli, D.; Spinace, E.V.; Fires, E.L. Cyclohexane oxidation continues to be a challenge. *Appl. Catal. A Gen.* **2001**, *211*, 1–17. [[CrossRef](#)]
6. Kirillov, A.M.; Haukka, M.; Guedes da Silva, M.F.C.; Pombeiro, A.J.L. Preparation and crystal structures of benzoylhydrazido- and-diazenidorhenium complexes with N,O-ligands and their catalytic activity towards peroxidative oxidation of cycloalkanes. *Eur. J. Inorg. Chem.* **2005**, *11*, 2071–2080. [[CrossRef](#)]
7. Gupta, S.; Kirillova, M.V.; Guedes da Silva, M.F.C.; Pombeiro, A.J.L.; Kirillov, A.M. Alkali metal directed assembly of heterometallic V_v/M (M = Na, K, Cs) coordination polymers: Structures, topological analysis, and oxidation catalytic properties. *Inorg. Chem.* **2013**, *52*, 8601–8611. [[CrossRef](#)] [[PubMed](#)]
8. Dias, S.S.P.; Kirillova, M.V.; André, V.; Kłak, J.; Kirillov, A.M. New tetracopper(II) cubane cores driven by a diamino alcohol: Self-assembly synthesis, structural and topological features, and magnetic and catalytic oxidation properties. *Inorg. Chem.* **2015**, *54*, 5204–5212. [[CrossRef](#)] [[PubMed](#)]
9. Fernandes, T.A.; Santos, C.I.M.; André, V.; Kłak, J.; Kirillova, M.V.; Kirillov, A.M. Copper(II) coordination polymers self-assembled from aminoalcohols and pyromellitic acid: Highly active precatalysts for the mild water-promoted oxidation of alkanes. *Inorg. Chem.* **2016**, *55*, 125–135. [[CrossRef](#)] [[PubMed](#)]
10. Kirillov, A.M.; Kirillova, M.V.; Pombeiro, A.J.L. Chapter one—Homogeneous multicopper catalysts for oxidation and hydrocarboxylation of alkanes. In *Advances in Inorganic Chemistry*; Rudi van, E., Colin, D.H., Eds.; Academic Press: Cambridge, MA, USA, 2013; Volume 65, pp. 1–31; ISBN: 0898-8838.

11. Long, J.L.; Liu, H.L.; Wu, S.J.; Liao, S.J.; Li, Y.W. Selective oxidation of saturated hydrocarbons using Au-Pd alloy nanoparticles supported on metal-organic frameworks. *ACS Catal.* **2013**, *3*, 647–654. [[CrossRef](#)]
12. Wang, L.; Zhao, S.; Liu, C.; Li, C.; Li, X.; Li, H.; Wang, Y.; Ma, C.; Li, Z.; Zeng, J. Aerobic oxidation of cyclohexane on catalysts based on twinned and single-crystal Au₇₅Pd₂₅ bimetallic nanocrystals. *Nano Lett.* **2015**, *15*, 2875–2880. [[CrossRef](#)] [[PubMed](#)]
13. Mohamed, M.M. Gold loaded titanium dioxide-carbon nanotube composites as active photocatalysts for cyclohexane oxidation at ambient conditions. *RSC Adv.* **2015**, *5*, 46405–46414. [[CrossRef](#)]
14. Carabineiro, S.A.C.; Martins, L.M.D.R.S.; Avalos-Borja, M.; Buijnsters, J.G.; Pombeiro, A.J.L.; Figueiredo, J.L. Gold nanoparticles supported on carbon materials for cyclohexane oxidation with hydrogen peroxide. *Appl. Catal. A Gen.* **2013**, *467*, 279–290. [[CrossRef](#)]
15. De Almeida, M.P.; Martins, L.M.D.R.S.; Carabineiro, S.A.C.; Lauterbach, T.; Rominger, F.; Hashmi, A.S.K.; Pombeiro, A.J.L.; Figueiredo, J.L. Homogeneous and heterogenised new gold C-scorpionate complexes as catalysts for cyclohexane oxidation. *Catal. Sci. Technol.* **2013**, *3*, 3056–3069. [[CrossRef](#)]
16. Martins, L.M.D.R.S.; Carabineiro, S.A.C.; Wang, J.; Rocha, B.G.M.; Maldonado-Hódar, F.J.; Latourrette de Oliveira Pombeiro, A.J. Supported gold nanoparticles as reusable catalysts for oxidation reactions of industrial significance. *ChemCatChem* **2017**, *9*, 1211–1221. [[CrossRef](#)]
17. Jiang, Y.X.; Su, T.M.; Qin, Z.Z.; Huang, G. A zinc sulfide-supported iron tetrakis (4-carboxyl phenyl) porphyrin catalyst for aerobic oxidation of cyclohexane. *RSC Adv.* **2015**, *5*, 24788–24794. [[CrossRef](#)]
18. Feng, Z.; Xie, Y.J.; Hao, F.; Liu, P.L.; Luo, H.A. Catalytic oxidation of cyclohexane to KA oil by zinc oxide supported manganese 5,10,15,20-tetrakis(4-nitrophenyl)porphyrin. *J. Mol. Catal. A Chem.* **2015**, *410*, 221–225. [[CrossRef](#)]
19. Mishra, G.S.; Alegria, E.C.B.; Martins, L.M.D.R.S.; Fraústo da Silva, J.J.R.; Pombeiro, A.J.L. Cyclohexane oxidation with dioxygen catalyzed by supported pyrazole rhenium complexes. *J. Mol. Catal. A Chem.* **2008**, *285*, 92–100. [[CrossRef](#)]
20. Martins, L.M.D.R.S.; de Almeida, M.P.; Carabineiro, S.A.C.; Figueiredo, J.L.; Pombeiro, A.J.L. Heterogenisation of a C-scorpionate feii complex on carbon materials for cyclohexane oxidation with hydrogen peroxide. *ChemCatChem* **2013**, *5*, 3847–3856. [[CrossRef](#)]
21. Devika, S.; Palanichamy, M.; Murugesan, V. Vapour phase oxidation of cyclohexane over CeAlPO-5 molecular sieves. *J. Mol. Catal. A Chem.* **2011**, *351*, 136–142. [[CrossRef](#)]
22. Anand, R.; Hamdy, M.S.; Hanefeld, U.; Maschmeyer, T. Liquid-Phase oxidation of cyclohexane over Co-TUD-1. *Catal. Lett.* **2004**, *95*, 113–117. [[CrossRef](#)]
23. Li, J.; Shi, Y.; Xu, L.; Lu, G.Z. Selective oxidation of cyclohexane over transition-metal-incorporated HMS in a solvent-free system. *Ind. Eng. Chem. Res.* **2010**, *49*, 5392–5399. [[CrossRef](#)]
24. Zhang, P.F.; Lu, H.F.; Zhou, Y.; Zhang, L.; Wu, Z.L.; Yang, S.Z.; Shi, H.L.; Zhu, Q.L.; Chen, Y.F.; Dai, S. Mesoporous MnCeO_x solid solutions for low temperature and selective oxidation of hydrocarbons. *Nat. Commun.* **2015**, *6*, 8446. [[CrossRef](#)] [[PubMed](#)]
25. Zabihi, M.; Khorasheh, F.; Shayegan, J. Supported copper and cobalt oxides on activated carbon for simultaneous oxidation of toluene and cyclohexane in air. *RSC Adv.* **2015**, *5*, 5107–5122. [[CrossRef](#)]
26. Aboelfetoh, E.F.; Pietschnig, R. Preparation, characterization and catalytic activity of MgO/SiO₂ supported vanadium oxide based catalysts. *Catal. Lett.* **2014**, *144*, 97–103. [[CrossRef](#)]
27. Liu, D.C.; Zhang, B.Q.; Liu, X.F.; Li, J. Cyclohexane oxidation over AFI molecular sieves: Effects of Cr, Co incorporation and crystal size. *Catal. Sci. Technol.* **2015**, *5*, 3394–3402. [[CrossRef](#)]
28. Masters, A.F.; Beattie, J.K.; Roa, A.L. Synthesis of a CrCoAPO-5(AFI) molecular sSieve and its activity in cyclohexane oxidation in the liquid phase. *Catal. Lett.* **2001**, *75*, 159–162. [[CrossRef](#)]
29. Zhao, R.; Ji, D.; Lv, G.M.; Qian, G.; Yan, L.; Wang, X.L.; Suo, J.S. A highly efficient oxidation of cyclohexane over Au/ZSM-5 molecular sieve catalyst with oxygen as oxidant. *Chem. Commun.* **2004**, *7*, 904–905. [[CrossRef](#)] [[PubMed](#)]
30. Modén, B.; Oliviero, L.; Dakka, J.; Santiesteban, J.G.; Iglesia, E. Structural and functional characterization of redox mn and co sites in alpo materials and their role in alkane oxidation catalysis. *J. Phys. Chem. B* **2004**, *108*, 5552–5563. [[CrossRef](#)]
31. Qian, G.; Ji, D.; Lu, G.M.; Zhao, R.; Qi, Y.X.; Suo, J.S. Bismuth-containing MCM-41: Synthesis, characterization, and catalytic behavior in liquid-phase oxidation of cyclohexane. *J. Catal.* **2005**, *232*, 378–385. [[CrossRef](#)]

32. Perkas, N.; Koltypin, Y.; Palchik, O.; Gedanken, A.; Chandrasekaran, S. Oxidation of cyclohexane with nanostructured amorphous catalysts under mild conditions. *Appl. Catal. A Gen.* **2001**, *209*, 125–130. [[CrossRef](#)]
33. Perkas, N.; Wang, Y.; Koltypin, Y.; Gedanken, A.; Chandrasekaran, S. Mesoporous iron-titania catalyst for cyclohexane oxidation. *Chem. Commun.* **2001**, *11*, 988–989. [[CrossRef](#)]
34. Zhou, L.P.; Xu, J.; Miao, H.; Wang, F.; Li, X.Q. Catalytic oxidation of cyclohexane to cyclohexanol and cyclohexanone over Co_3O_4 nanocrystals with molecular oxygen. *Appl. Catal. A Gen.* **2005**, *292*, 223–228. [[CrossRef](#)]
35. Conte, M.; Liu, X.; Murphy, D.M.; Whiston, K.; Hutchings, G.J. Cyclohexane oxidation using Au/MgO: An investigation of the reaction mechanism. *Phys. Chem. Chem. Phys.* **2012**, *14*, 16279–16285. [[CrossRef](#)] [[PubMed](#)]
36. Wu, M.Z.; Zhan, W.C.; Guo, Y.L.; Guo, Y.; Wang, Y.S.; Wang, L.; Lu, G.Z. An effective Mn-Co mixed oxide catalyst for the solvent-free selective oxidation of cyclohexane with molecular oxygen. *Appl. Catal. A Gen.* **2016**, *523*, 97–106. [[CrossRef](#)]
37. Aboelfetoh, E.F.; Pietschnig, R. Preparation and catalytic performance of Al_2O_3 , TiO_2 and SiO_2 supported vanadium based-catalysts for C–H activation. *Catal. Lett.* **2009**, *127*, 83–94. [[CrossRef](#)]
38. Masteri-Farahani, M. Investigation of catalytic activities of new heterogeneous molybdenum catalysts in epoxidation of olefins. *J. Mol. Catal. A Chem.* **2010**, *316*, 45–51. [[CrossRef](#)]
39. Kim, P.S.; Kim, M.K.; Cho, B.K.; Nam, I.S. Autocatalytic synergism observed during lean- NO_x reduction with a bifunctional reductant over Ag/ Al_2O_3 catalyst. *J. Catal.* **2012**, *292*, 44–52. [[CrossRef](#)]
40. Ramanathan, A.; Hamdy, M.S.; Parton, R.; Maschmeyer, T.; Jansen, J.C.; Hanefeld, U. Co-TUD-1 catalysed aerobic oxidation of cyclohexane. *Appl. Catal. A Gen.* **2009**, *355*, 78–82. [[CrossRef](#)]
41. Tolman, C.A.; Druliner, J.D.; Nappa, M.J.; Herron, C. *Activation and Functionalisation of Alkanes*; Hill, C.L., Ed.; Wiley: New York, NY, USA, 1989.
42. Cazzanelli, E.; Kuzmin, A.; Mariotto, G.; Mironova-Ulmane, N. Study of vibrational and magnetic excitations in $\text{Ni}_c\text{Mg}_{1-c}\text{O}$ solid solutions by Raman spectroscopy. *J. Phys. Condens. Matter* **2003**, *15*, 2045. [[CrossRef](#)]
43. Mironova-Ulmane, N.; Kuzmin, A.; Steins, I.; Grabis, J.; Sildos, I.; Pārs, M. Raman scattering in nanosized nickel oxide NiO . *J. Phys. Conf. Ser.* **2007**, *93*, 012039. [[CrossRef](#)]
44. Wu, L.B.; Jiao, D.M.; Wang, J.A.; Chen, L.F.; Cao, F.H. The role of MgO in the formation of surface active phases of $\text{CoMo}/\text{Al}_2\text{O}_3$ -MgO catalysts for hydrodesulfurization of dibenzothiophene. *Catal. Commun.* **2009**, *11*, 302–305. [[CrossRef](#)]
45. Wang, G.X.; Shen, X.P.; Horvat, J.; Wang, B.; Liu, H.; Wexler, D.; Yao, J. Hydrothermal synthesis and optical, magnetic, and supercapacitance properties of nanoporous cobalt oxide nanorods. *J. Phys. Chem. C* **2009**, *113*, 4357–4361. [[CrossRef](#)]
46. Jiang, J.; Li, L.C. Synthesis of sphere-like Co_3O_4 nanocrystals via a simple polyol route. *Mater. Lett.* **2007**, *61*, 4894–4896. [[CrossRef](#)]
47. Liu, Q.; Wang, L.C.; Chen, M.; Cao, Y.; He, H.Y.; Fan, K.N. Dry citrate-precursor synthesized nanocrystalline cobalt oxide as highly active catalyst for total oxidation of propane. *J. Catal.* **2009**, *263*, 104. [[CrossRef](#)]
48. Li, J.; Lu, G.Z.; Wu, G.S.; Mao, D.S.; Guo, Y.L.; Wang, Y.Q.; Guo, Y. The role of iron oxide in the highly effective Fe-modified Co_3O_4 catalyst for low-temperature CO oxidation. *RSC Adv.* **2013**, *3*, 12409–12416. [[CrossRef](#)]
49. Liu, F.D.; He, H.; Ding, Y.; Zhang, C.B. Effect of manganese substitution on the structure and activity of iron titanate catalyst for the selective catalytic reduction of NO with NH_3 . *Appl. Catal. B Environ.* **2009**, *93*, 194–204. [[CrossRef](#)]
50. Wang, X.Y.; Kang, Q.; Li, D. Catalytic combustion of chlorobenzene over MnO_x - CeO_2 mixed oxide catalysts. *Appl. Catal. B Environ.* **2009**, *86*, 166–175. [[CrossRef](#)]
51. Zhang, W.; Tay, H.L.; Lim, S.S.; Wang, Y.S.; Zhong, Z.Y.; Xu, R. Supported cobalt oxide on MgO: Highly efficient catalysts for degradation of organic dyes in dilute solutions. *Appl. Catal. B Environ.* **2010**, *95*, 93–99. [[CrossRef](#)]
52. Riva, R.; Miessner, H.; Vitali, R.; Del Piero, G. Metal-support interaction in Co/SiO_2 and Co/TiO_2 . *Appl. Catal. A Gen.* **2000**, *196*, 111–123. [[CrossRef](#)]
53. Todorova, S.; Kolev, H.; Holgado, J.P.; Kadinov, G.; Bonev, C.; Pereñíguez, R.; Caballero, A. Complete n-hexane oxidation over supported Mn–Co catalysts. *Appl. Catal. B Environ.* **2010**, *94*, 46–54. [[CrossRef](#)]

54. Sun, C.H.; Berg, J.C. A review of the different techniques for solid surface acid-base characterization. *Colloid Interface Sci.* **2003**, *105*, 151–175. [[CrossRef](#)]
55. Skofronick, J.G.; Toennies, J.P.; Traeger, F.; Weiss, H. Helium atom scattering studies of the structure and vibrations of H₂ physisorbed on MgO(001) single crystals. *Phys. Rev. B* **2003**, *67*, 035413. [[CrossRef](#)]
56. Mei, J.; Zhao, S.J.; Xu, H.M.; Qu, Z.; Yan, N.Q. The performance and mechanism for the catalytic oxidation of dibromomethane (CH₂Br₂) over Co₃O₄/TiO₂ catalysts. *RSC Adv.* **2016**, *6*, 31181–31190. [[CrossRef](#)]
57. Li, C.; Domen, K.; Maruya, K.; Onishi, T. Dioxygen adsorption on well-outgassed and partially reduced cerium oxide studied by FT-IR. *J. Am. Chem. Soc.* **1989**, *111*, 7683–7687. [[CrossRef](#)]
58. Huang, H.; Gu, Y.F.; Zhao, J.; Wang, X.Y. Catalytic combustion of chlorobenzene over VO_x/CeO₂ catalysts. *J. Catal.* **2015**, *326*, 54–68. [[CrossRef](#)]
59. Liang, H.; Hong, Y.X.; Zhu, C.Q.; Li, S.H.; Chen, Y.; Liu, Z.L.; Ye, D.Q. Influence of partial Mn-substitution on surface oxygen species of LaCoO₃ catalysts. *Catal. Today* **2013**, *201*, 98–102. [[CrossRef](#)]
60. Xie, X.W.; Li, Y.; Liu, Z.Q.; Haruta, M.; Shen, W.J. Low-temperature oxidation of CO catalysed by Co₃O₄ nanorods. *Nature* **2009**, *458*, 746–749. [[CrossRef](#)] [[PubMed](#)]
61. Qiu, X.P.; Yu, J.S.; Xu, H.M.; Chen, W.X.; Hu, W.; Chen, G.L. Interfacial effects of the Cu₂O nano-dots decorated Co₃O₄ nanorods array and its photocatalytic activity for cleaving organic molecules. *Appl. Surf. Sci.* **2016**, *382*, 249–259. [[CrossRef](#)]
62. Sheldon, R.A.; Wallau, M.; Arends, I.W.C.E.; Schuchardt, U. Heterogeneous catalysts for liquid-phase oxidations: Philosophers' stones or Trojan horses? *Acc. Chem. Res.* **1998**, *31*, 485–493. [[CrossRef](#)]
63. Wang, Q.; Peng, Y.; Fu, J.; Kyzas, G.Z.; Billah, S.M.R.; An, S.Q. Synthesis, characterization, and catalytic evaluation of Co₃O₄/γ-Al₂O₃ as methane combustion catalysts: Significance of Co species and the redox cycle. *Appl. Catal. B Environ.* **2015**, *168–169*, 42–50. [[CrossRef](#)]
64. Wen, Y.; Potter, O.E.; Sridhar, T. Uncatalysed oxidation of cyclohexane in a continuous reactor. *Chem. Eng. Sci.* **1997**, *52*, 4593–4605. [[CrossRef](#)]
65. Shul'pin, G.B. Metal-catalyzed hydrocarbon oxygenations in solutions: The dramatic role of additives: A review. *J. Mol. Catal. A Chem.* **2002**, *189*, 39–66. [[CrossRef](#)]



© 2017 by the authors. Licensee MDPI, Basel, Switzerland. This article is an open access article distributed under the terms and conditions of the Creative Commons Attribution (CC BY) license (<http://creativecommons.org/licenses/by/4.0/>).